JOURNAL OF GUIDANCE, CONTROL, AND DYNAMICS
Vol. 24, No. 5, September–October 2001

Comparing Model Simulations with Flight Performance of Spacecraft Deployable Appendages

Norman S. Lomas*
INTELSAT, Palo Alto, California 94303

Most spacecraft depend on the successful deployments of solar power arrays and communications antennas to carry out their missions. Telemetry recorded during flight deployments is closely watched for positive results. The tools and methodology that are used to interpret the characteristic deployment signatures recorded in telemetry from spacecraft attitude control sensors are described in this paper. These tools are then applied to a real-life example. Deployment signatures from INTELSAT VII communications satellites are compared with flight simulation results to learn why antenna deployments were faster than predicted and why attitude disturbances caused by solar wing deployments were always greater than expected. Sensitivities of the flight deployment signatures to the inertial effects of fluids in the propellant tanks and small alignment errors are examined to help distinguish between normal and abnormal performance.

I. Introduction

FOLDING solar arrays, deployable communications antennas, and instrument booms are used by spacecraft configuration designers to achieve tight packaging requirements inside a launch vehicle's fairing. Figure 1 shows the placement of the deployable appendages on a typical commercial communications satellite. The box-shaped, central body houses the payload and supporting subsystems; lightweight solar wings and communications antennas extend from the four sides. During launch, the solar wings are folded on the north and south faces of the box, and the large dish reflectors are stowed to the east and west sides.

Gyros and optical sensors of the satellite's attitude control subsystem can be used to eavesdrop on the deployment of an antenna or solar wing. For example, the output of a roll gyro during a solar wing deployment might look like the waveform shown in Fig. 1. The gyro measures the rotation of the central body about the roll axis as the solar wing unfolds. The time history of the roll angle is like the signature of the deployment and, like a handwriting sample, has much to say about its subject.

Section II of this paper presents a method for extracting detailed system performance information from the flight deployment signatures. The process starts with a dynamic simulation model of the satellite and deployable appendage. Controlled by a set of parameters, the model is adjusted and the simulation rerun in an iterative process to reproduce the flight results as closely as possible.

Section III illustrates some practical applications of deployment modeling methods in the case of the INTELSAT VII. The antennas and solar wings[1] of eight I-VII communications satellites were successfully deployed in flight. However, some features of the deployment signatures raised concerns about deployment load margins and performance repeatability. Antenna deployments tended to have higher rates than expected; there were large roll disturbances during solar wing deployments, and the curious variability of the residual displacements was also a puzzle. The deployment simulations helped to explain the signature data and to provide information to make corrective actions for future space deployment systems.

The open literature contains some excellent design studies where deployment simulation modeling is supported by laboratory tests of flightlike hardware.[2–4] The present study differs from these works in its use of flight telemetry to make detailed performance evaluations. Comparing flight dynamic telemetry with simulation results provides a real-world test for the modeling methodology because it describes the performance under true operational conditions, away from the pervasive effects of gravity and air loading in an Earth-bound laboratory experiment.

Received 26 June 2000; revision received 2 April 2001; accepted for publication 7 April 2001.

*Principal Engineer, Space Programs Management. Senior Member AIAA.

II. Deployment Dynamic Modeling

The topology of a typical deployment model is like a tree whose branches are rigid bodies connected by mechanical joints. One of the rigid bodies represents the free- floating central body of the satellite, and the other bodies are the folding segments of the deployable appendage(s). Rigid-body modeling implies that the stiffness of the structural members (solar panels, booms) is large in comparison with the mechanical members (hinges, etc.). This is often the case. However, furlable appendages are not so simple to model and often require special treatment of flexible-body effects.[5]

Modeling of liquid propellants and the kinematic constraints associated with the mechanisms[6] create other challenges in building a high-fidelity satellite deployment simulation model. How these challenges were met in a real-life situation is described in Sec. III.

Multibody Models

Figure 2 shows the basic plan and connectivity of antenna and solar array deployment analysis models. The former, in Fig. 2a, consists of three bodies: the satellite central body A, the antenna B, and a small folding holddown member C. The more complex model for solar wing deployments is shown in Fig. 2b. It is composed of six bodies: one representing the central body A, one each for the yoke and solar panels (B–E), and one representing the flexibility of another appendage G on the opposite side of the central body.

Even the simple two-body problem does not have a closed-form solution. However, computer codes are available to take a dynamic model, assemble and integrate the equations of motion, and solve for the time variation of all degrees of freedom. ADAMS (Mechanical Dynamics, Inc.) and ProE/Mechanica (Parametric Technology Corporation) are two commercial software packages for analyzing the dynamics of mechanical systems. In this study, the Autolev program[7] was used to generate most of the computer code, while allowing the user to add subroutines describing constraints and torques at the hinge joints.

Single-Degree-of-Freedom Model

The textbook problem of a single-degree-of-freedom torsional oscillator is a useful analogy for many space antenna deployments. This is because the mass of the antenna is small compared with the central body, and the friction in the hinge is also low.

Therefore, suppose a body with rotational inertia I moves about a frictionless, fixed hinge attached to a linear torsion spring of stiffness K. Assume that the spring has been wound so that it applies a torque T in the initial rest position. If the body is released from rest with

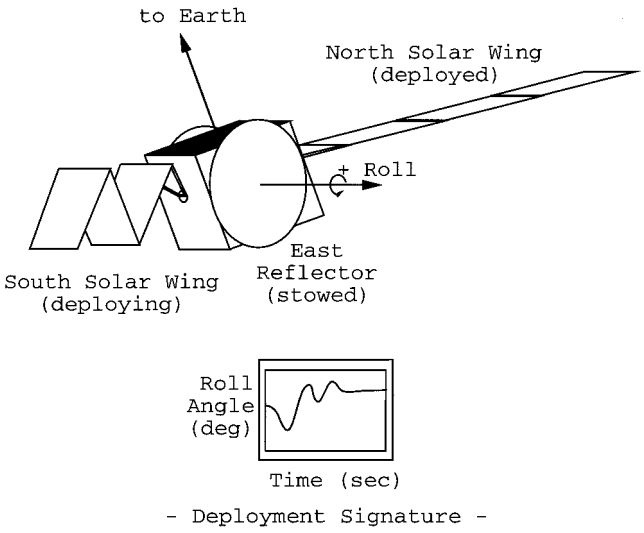

Fig. 1 Monitoring solar wing deployments on a typical commercial communications satellite.

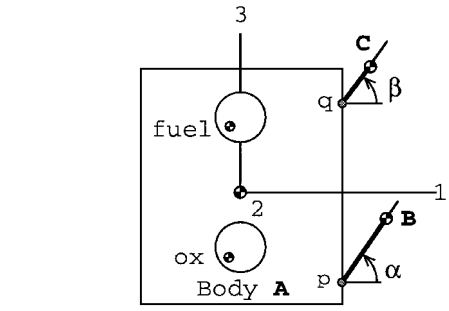

a) Antenna and holddown: modeled with residual propellants

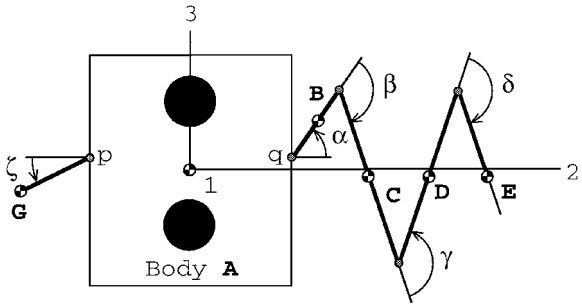

b) Solar wing: modeled with full propellant tanks

Fig. 2 Elements of deployment simulation models: 1–3, body-fixed coordinates; ⊙, hingeline; and ◔, mass center.

no initial velocity, the time required for it to rotate through an angle α is given by

$$t = (1/\omega)\cos^{-1}[1 - (K/T)\alpha] \tag{1}$$

where $\omega^2 = K/I$.

Space deployment hinges usually have built-in latches or stops to limit their range of travel. Structural loads produced when the body reaches the end of travel can be computed by considering the energy exchange between the torsional oscillator and a linear capture spring whose stiffness $\bar{K}$ represents the elasticity of the latch mechanism and supporting structure. The peak bending moment M_p is given by

$$M_p = \bar{K}\varepsilon \tag{2}$$

where

$$\varepsilon = \sqrt{(K/\bar{K})\alpha(2T/K - \alpha)}$$

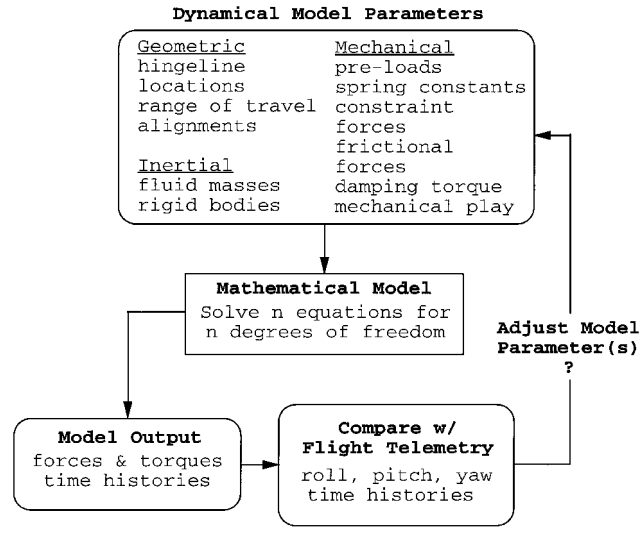

Fig. 3 Iterative process for correlating model predictions with flight results.

Model Correlation with Flight Data

A process for correlating deployment analyses with flight data is shown in the block diagram of Fig. 3. It starts with a model of the dynamic system with n degrees of freedom and is described by a set of geometric, inertial, and mechanical parameters. The model is mathematically described by a system of n simultaneous equations for the rotational and translational degrees of freedom. Solving the equations subject to the predeployment initial conditions gives a set of n time histories from which the internal loads also can be computed.

The analyst decides how well the time histories of the roll, pitch, and yaw disturbances compare with the flight telemetry. If the results are not satisfactory, selected parameters of the model are readjusted. When the model's degrees of freedom are strongly coupled to each other through a small subset of parameters, several iterations may be needed to reach convergence. At each step, a new solution is obtained, and the results are compared with the flight data. The process is complete when the model has been tuned to the desired accuracy.

The subset of model parameters that require retuning are the parameters that may have been out of tolerance, or otherwise inaccurately expressed in the original model, for example, spring settings, mass properties, mechanical play, and alignments. Their existence may signify anomalous flight performance, weak modeling assumptions, or just performance under abnormal conditions.

III. Results of INTELSAT VII Flight Data Analyses

The analysis process outlined in Sec. II is applied to the flight deployments of INTELSAT VII antennas and solar array wings in this section. A brief description of the satellite is given first, followed by discussions of the findings of this study.

About INTELSAT VII

INTELSAT VII (or I-VII) is a series of communications satellites owned by the INTELSAT organization. There are six I-VII spacecraft, and two somewhat larger I-VIIAs, operating in geosynchronous orbit.

INTELSAT VII solar wings and antennas were deployed separately in flight. Their masses are compared with the satellite launch mass in Table 1. Notice that no appendage has a mass greater than 1–2% of the total satellite mass.

The satellite's mechanical design and mission plan are reflected in the deployment models. Important features of these models include 1) solar panels and reflectors treated as rigid bodies, 2) spring-driven deployment hinges (a latch mechanism limits the range of travel of each hinge), 3) kinematic cables to synchronize the movement of the solar panels by linking all hingelines to the rotation of the root hinge, 4) a viscous rotary damper installed on the root hinge to control the rate of solar wing deployment, and 5) control thrusters disabled before each deployment, so that there are no external torques acting on the system.

Table 1 Mass and deployment range of travel of I-VII/I-VIIA deployable appendages

Property	Mass, kg	Range of travel, deg
I-VII launch mass	3400–3700	——
I-VIIA launch mass	4200–4700	——
I-VII solar wing	56	90 (yoke), 180 (panel)
I-VIIA solar wing	75	90 (yoke), 180 (panel)
4-GHz reflector	15	62
4-GHz holddown	2	54
6-GHz reflector	9	59
6-GHz holddown	2	77

Table 2 Antenna reflector deployment summary

		4-GHz reflector		6-GHz reflector	
Spacecraft	Propellant mass fraction	Deploy time, s	Pitch offset, deg	Deploy time, s	Pitch offset, deg
I-VII					
701	0.32	5.6	−0.81	2.7	0.21
702	0.32	6.2	−0.84	2.8	0.22
703	0.25	6.0	−0.89	2.9	0.22
704	0.24	6.4	−0.87	3.3	0.22
705	0.26	5.1	−0.87	3.3	0.22
709	0.29	6.9	−0.96	3.5	0.20
I-VIIA					
706	0.31	6.0	−0.75	3.3	0.20
707	0.29	6.2	−0.72	2.9	0.19
Frictionless limit		6.7		3.5	

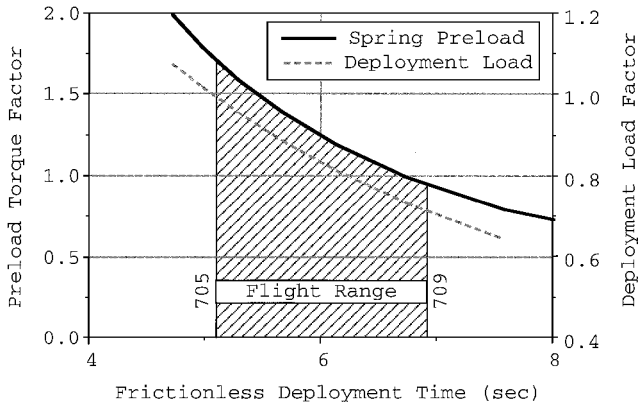

Fig. 4 Relating the predicted deployment time of the 4-GHz reflector to the preload torque and peak deployment loads.

Antenna Deployments

A summary of INTELSAT VII antenna deployments is given in Table 2. The flight data include the time to deploy and the net change in the satellite's pitch attitude resulting from the deployment.

A close look at the numbers in Table 2 raises some interesting questions. For example, the frictionless limits are the deployment times predicted by Eq. (1) with nominal spring settings. They are the shortest possible deployment times for a given set of spring torque parameters. However, the flight deployment times are shorter than the frictionless limit in every case except INTELSAT 709.

Another puzzle is the curious variability in the pitch attitude offset from flight to flight. This is surprising because the six I-VII spacecraft were outwardly identical.

Effect of Hinge Spring Settings on Deployment Rates

The problem of the antenna deployment rates can be tackled with the aid of Eqs. (1) and (2). Equation (1) says that the frictionless deployment time depends on two mechanical parameters: the hinge spring constant and the torque setting. Figure 4 shows the relationship between the frictionless deployment time, preload torque T, and peak deployment loads. On the vertical axes, the spring torque and the loads are normalized with respect to their nominal values.

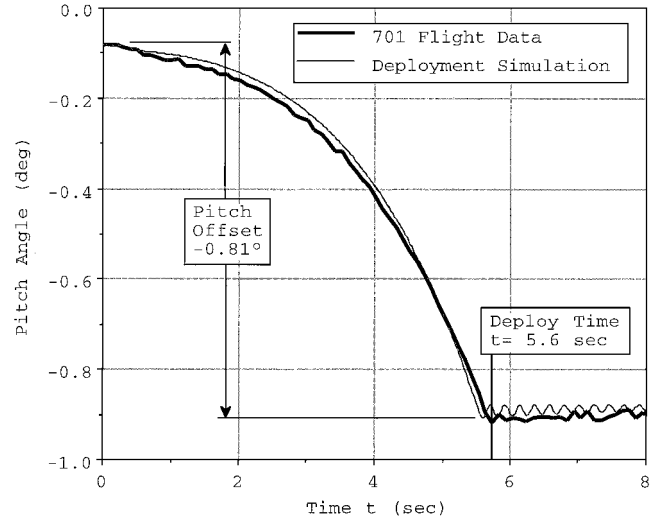

Fig. 5 Signature of 4-GHz reflector deployment in the pitch attitude of INTELSAT 701.

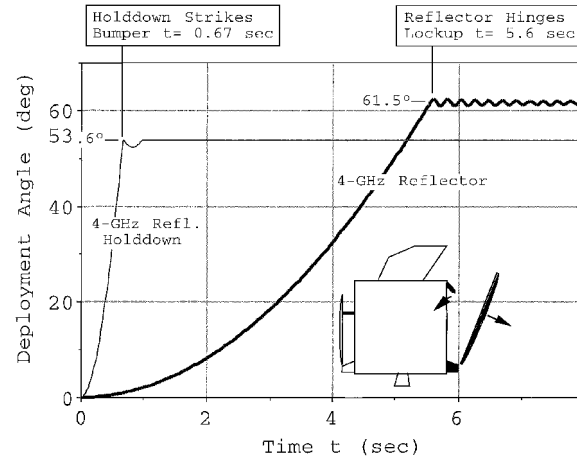

Fig. 6 Predicted movement of the 4-GHz reflector and holddown.

Notice that spring settings as great as 1.7 times the nominal value are needed to produce the high rates observed in flight.

To verify this result, a full deployment simulation was run using the dynamic model shown in Fig. 2a. The time history of the pitch attitude computed here is plotted in Fig. 5 along with the flight deployment signature of the INTELSAT 701 4-GHz reflector. The predicted deployment time is in good agreement with the telemetry only because the torque of the deployment hinge springs was increased well above the nominal values. Figure 6 shows the predicted movement of the 4-GHz reflector and holddown after tuning the model to match the flight deployment time. The holddown was modeled with impact-absorbing stops to add realism to the simulation.

The most likely cause of the fast antenna deployments was a systematic error in resetting the deployment springs when the reflectors were installed on the satellite for the final time. The deployment load curve in Fig. 4 indicates that the highest loads sustained by the 4-GHz reflector support system occurred on INTELSAT 705. These loads probably exceeded the design qualification limit by 50%.

Effect of the Propellants on the Pitch Offset

INTELSAT VII antenna deployments took place just after the satellite completed a series of orbit-raising maneuvers. Evidence from the deployment signatures suggests that the fluids remaining in the propellant tanks had not reached a state of inertial equilibrium with the satellite body at the time the first reflector was deployed.

The role of the fluids in the antenna deployments is underscored by noting how well the magnitude of the pitch offset tracks with propellant mass fraction in Table 2. Physical coupling of the fluids

to the central body is controlled by surface tension devices inside the propellant tanks. These are designed to trap the fluids and channel them to the tank outlet ports for orbital station-keeping maneuvers.

A qualitative understanding of the fluid–inertial coupling can be obtained by calculating the dimensionless Weber number, *We*. The Weber number[8,9] is the ratio of deployment inertial forces to the fluid surface tension forces, that is,

$$We = \frac{\text{inertial forces}}{\text{surface tension forces}} = \frac{U}{\sqrt{\sigma/\rho R}} \tag{3}$$

where U is a characteristic velocity, R the length of the fluid mass, σ its surface tension coefficient, and ρ its density. With the tank radius R as the characteristic length, the Weber number for INTELSAT VII reflector deployments is about 10^{-2}.

The dominance of surface tension forces over inertial forces greatly simplifies the treatment of the fluids in the dynamic model for antenna deployments. It means that fluid masses that are already in good contact with the tank walls are likely to remain so during the few seconds of a deployment. For modeling purposes, these fluids may be included with the rigid-body properties of the central body.

Three hypothetical propellant configurations were selected for study to place some bounds on the pitch offset magnitude. INTELSAT 701 mass properties were used in all of these calculations, and the results are shown in Fig. 7. The horizontal lines labeled $M = 0$ describe the case of empty tanks (or zero inertial coupling) and provide an upper bound on the pitch offset. All of the flight data lie to one side of these lines, as they should. Horizontal lines labeled $r = 0$ describe the case where the fluid mass centers are located at the geometric centers of the tanks. The results do not make a good match with INTELSAT 701 data, suggesting that it was not a good guess. Finally, the curves labeled $r/R = 0.7$ illustrate the sensitivity of the pitch offset to the β coordinate when the fluids are displaced

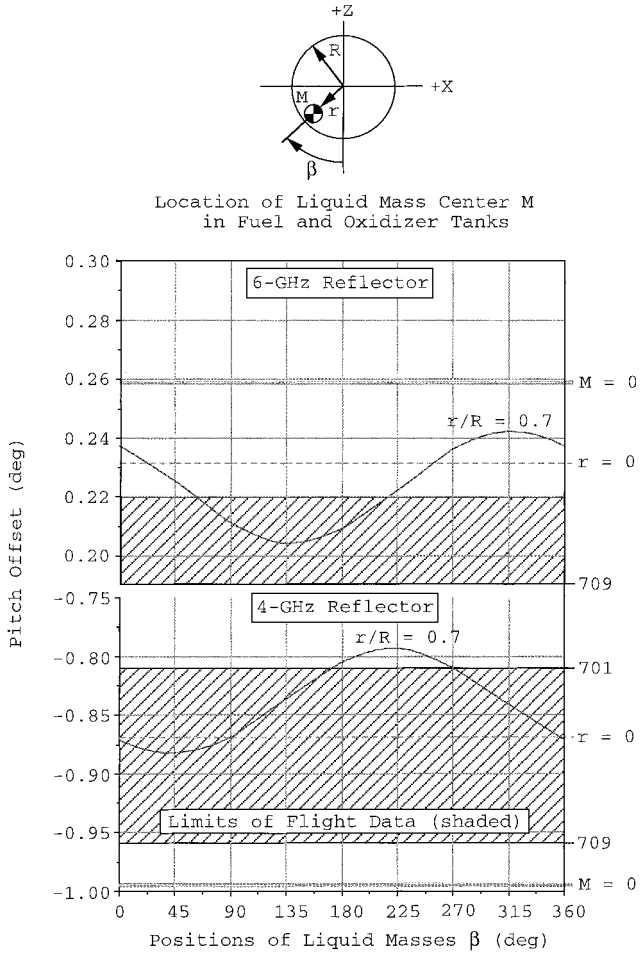

Fig. 7 Sensitivity of the pitch offset to propellant mass locations for antenna deployments.

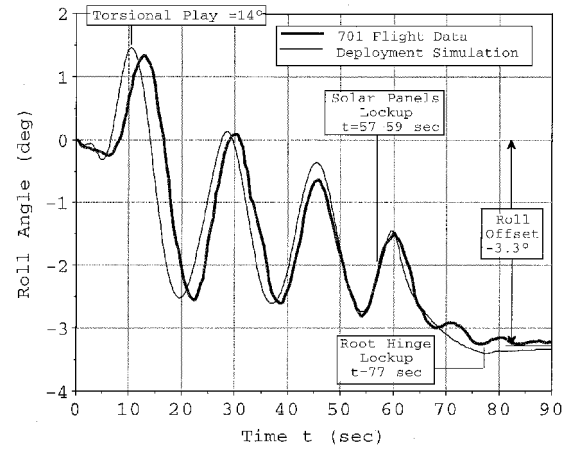

Fig. 8 Signature of the north solar wing deployment in the roll attitude of INTELSAT 701.

from the tank centers. For simplicity, the fuel and oxidizer were treated as separate spherical masses whose clock positions inside the tanks are identical (Fig. 2a).

In Table 2, larger propellant mass fractions usually go with smaller pitch offset angles. INTELSAT 709, however, makes an interesting exception to the rule. This satellite had both the largest and smallest offset angles of the I-VII population. The 4-GHz reflector deployment ended with a pitch offset that even approached the empty-tank limit ($M = 0$). However, 709 also had the third largest propellant mass fraction of the six I-VII spacecraft. The inconsistency here might be explained if the fluid in the 709 tanks was not well coupled to the central body during the first deployment. Hours later, the steady action of surface tension forces could have gathered stray fluids into closer contact with the tank walls, resulted in a comparatively small pitch offset for the 6-GHz reflector deployment.

Solar Array Deployments

Solar array deployments took place 2–3 h after the INTELSAT VII launch. The north solar wing was always deployed first, followed about 30 min later by the south wing. The deployments were best observed in the response of the satellite's roll attitude. The deployment signature of the INTELSAT 701 north solar wing in Fig. 8 is a typical example and illustrates three important indicators of deployment performance. One is the deployment time, which is estimated from the span of the roll oscillation. In this case, the time was about 77 s, but all deployments ranged from 60 to 100 s, depending on the temperature of the silicone fluid in the deployment damper. Another indicator, related to deployment loads, is the magnitude of the roll excursion at the first peak of the roll transient waveform. The third indicator is the magnitude of the roll offset that resulted from the deployment. The performance indicators are discussed in more detail in the next two sections.

Sensitivity of Deployment Loads to Mechanical Play

The deployment loads are directly related to the action of the deployment damper. Close attention to modeling the damping torque was necessary to calculate the flight loads associated with the deployment signatures. Model parameters that control the damping torque were adjusted within design tolerances to make the predictions match the flight data as seen in Fig. 8. For example, the coefficients of an empirical expression for the damping rate were adjusted for temperature to give the model the same deployment time as the flight solar wing. However, this had little effect on deployment loads. Instead, by examining the sensitivity of the loads to parameter variations, it was discovered that the mechanical play between the damper body and the yoke was the key parameter. In fact, it controls the amplitude of the roll disturbance. With no mechanical play, the INTELSAT 701 model predicted a peak roll excursion of only +0.1 deg, vs a measured value of +1.4 deg. Choosing 14 deg of mechanical play gave the best fit to the flight data and is consistent with observations from ground deployment tests of the yoke alone, before assembly with the solar panels.

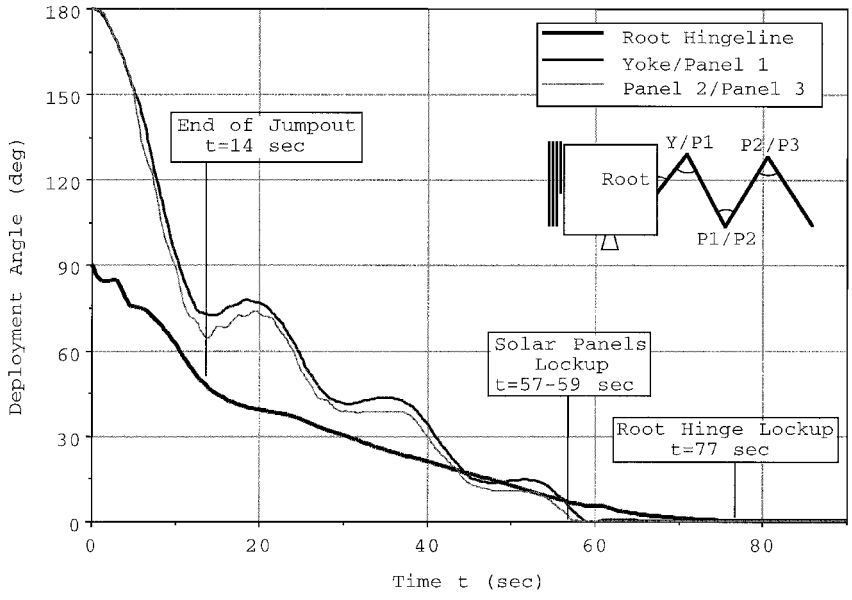

Fig. 9 Predicted motion of north solar wing hingelines.

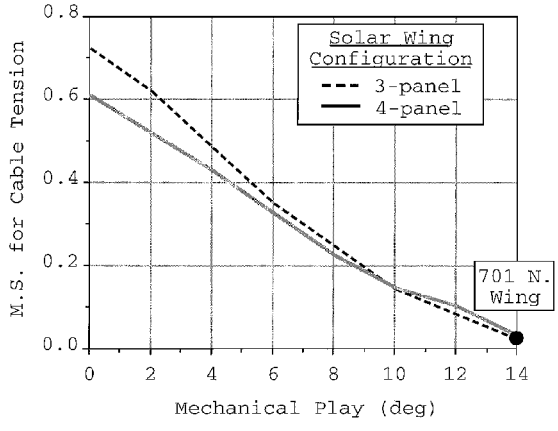

Fig. 10 Effect of mechanical play on the tensile MS of the yoke kinematic cable.

Maximum deployment loads occurred during the so-called jumpout phase, when a rapid redistribution of energy takes place as the solar wing starts unfolding. The jumpout phase lasts about as long as it takes for the damper and kinematic cables to become fully engaged in the movement of the solar panels and yoke. For example, in Fig. 8, jumpout begins with the release of the solar wing and ends near the time of the peak roll excursion. Figure 9 shows the predicted movement of three of the hingelines during deployment; notice that the jumpout is followed by another phase of motion, the rate-controlled phase, which ends with the lockup of the last hingeline. The deployment hinges move quickly through half their total range of travel during jumpout. Under rate control, the movement is slower and more uniform.

The margins of safety for flight deployment loads were reduced by the effect of mechanical play. For example, the most highly loaded segment of the kinematic cable system runs along the side of the yoke. Let P be the peak tensile load during deployment, and Pr be the cable proof load used in workmanship testing. The margin of safety (MS) can be defined as

$$\mathrm{MS} = P_r/P - 1 \tag{4}$$

Figure 10 shows the cable's MS for a tensile load as a function of the mechanical play for solar wing configurations of three and four panels. The graph shows that the predicted MS is a comfortable 0.60 with no mechanical play, but approaches zero in the simulation of the INTELSAT 701 north wing deployment.

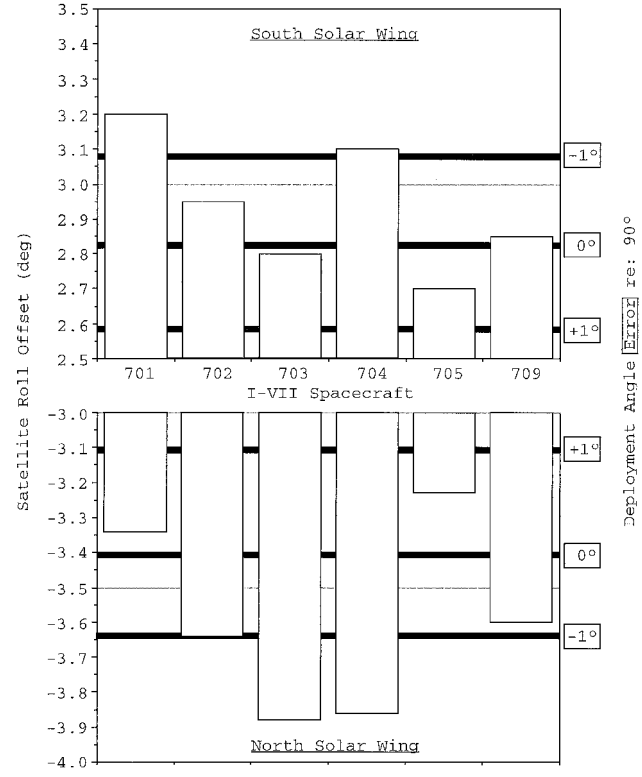

Fig. 11 Effect of solar wing alignment error on the satellite roll offset.

Effect of Solar Wing Alignments on the Roll Offset

Deployment of a solar wing leaves the satellite body with a net rotational displacement about the roll axis in the direction opposite from the root hinge. Like the pitch offset resulting from antenna deployments, the roll offset also exhibited variability from one flight to the next, but it was not so sensitive to the propellants because the tanks were almost full at this early stage of the mission. In fact, the alignment of the deployed solar wing was the single parameter controlling the variation of the roll offset.

The alignment requirement for an I-VII or I-VIIA solar wing was 90 ± 1 deg relative to the mounting plane of the root hinge. To see whether this requirement was achieved in practice, consider Fig. 11, where roll offset data from all I-VII solar wing deployments are plotted in the form of a bar chart. The dark bands on the chart are associated with the alignment errors labeled at right. A positive error

means that the solar wing is underdeployed, whereas a negative error means that the deployment went beyond the 90-deg position. For example, the INTELSAT 701 south wing is overdeployed by about 1 deg, and the north wing is just slightly underdeployed. Figure 11 indicates that the ±1-deg alignment limits were achieved in 8 of 12 flight cases. The solar wings were slightly overdeployed in the remaining four cases.

IV. Conclusions

Valuable information about the performance of spacecraft deployment mechanisms can be obtained from the characteristic signatures of deployments recorded by attitude control sensors. Section II of this paper described a method for extracting information from the deployment signatures; Sec. III demonstrated its practical application using INTELSAT VII solar array and antenna deployments for illustration.

Analysts try to unlock the secrets of the flight deployment signatures using dynamic models of the spacecraft and deployable appendage. Not surprisingly, models that started with nominal geometric, inertial, and mechanical properties quickly faltered in attempting to reproduce the INTELSAT VII flight signature plots. A few parameters of each model had to be adjusted to achieve good correlation with the flight data. Some of these parameters were linked to the performance of the deployment mechanisms, whereas others were not.

For example, the unexpectedly high deployment rates of INTELSAT VII communications reflectors were traced to a single model parameter, the deployment spring preload. Misadjustment of the springs on the flight hinges was the likely source of the high rates.

Solar wing deployment analyses identified an important mechanical parameter that had been overlooked earlier. This was the mechanical play between the body of the deployment damper and the yoke. Only mechanical play can explain the large excursions in the satellite's roll attitude that were seen in the flight deployment signatures.

Reliable estimates of deployment loads can be obtained from dynamic models that are correlated with the flight signatures. In one flight case, the loads on the hinges and support structure of an INTELSAT VII antenna probably reached design qualification limits. Load margins on critical parts of the solar wings, including the deployment damper and kinematic cable system, were reduced by the presence of the mechanical play.

Finally, two prominent features of the deployment signatures were not indicative of mechanical performance, but instead reflected the sensitivity of the spacecraft's postdeployment attitude to other factors. The variation of the pitch offset after antenna deployments depended on the configuration of the fluids in the propellant tanks; the roll offset variation after solar wing deployments was indicative of the final alignments of the wings themselves.

References

[1] Celli, J., Lomas, N., Pollard, H., and Totah, N., "INTELSAT VII Solar Array Electrical and Mechanical Design," *Proceedings of the 13th AIAA International Communications Satellite Systems Conference*, AIAA, Washington, DC, 1990, pp. 34–41.

[2] Marczyk, J., Tempesta, A., and Vilanova, J., "Modelling, Simulation and Control of In-Orbit Deployment of a Large Reflector: A Multi-Body Approach with ESA-Midas," *Proceedings of the 2nd International Conference on Dynamics and Control of Structures in Space*, Computational Mechanics Publishers, Southampton, England, U.K., 1993, pp. 3–31.

[3] Ueba, M., "Satellite Dynamics During Deployment of a Large Flexible Antenna Reflector," *Proceedings of 16th International Symposium on Space Technology and Science*, Vol. 1, AGNE Publishing, Inc., Tokyo, 1988, pp. 639–642.

[4] Meguro, A., and Mitsugi, J., "Ground Verification of Deployment Dynamics of Large Deployable Structures," *Journal of Spacecraft and Rockets*, Vol. 29, No. 6, 1992, pp. 835–841

[5] Bjorset, L. E., Krabberod, J., and Siversten, O. I., "Detailed Modeling and Dynamic Simulation of the Deployment of the MBB Unfurlable Antenna UMA," *2nd International Conference on Dynamics and Control of Structures in Space*, Computational Mechanics Publishers, Southampton, England, U.K., 1993, pp. 93–106.

[6] Banerjee, A. K., Barba, P. M., Furumoto, N., and Wie, B., "Modeling and Simulation of Spacecraft Solar Array Deployment," *Journal of Guidance, Control, and Dynamics*, Vol. 9, No. 5, 1986, pp. 593–598; also AIAA Paper 86-2122, Jan. 1986.

[7] Kane, T., and Levinson, T., *Dynamics Online: Theory and Implementation with Autolev*, Online Dynamics, Inc., Sunnyvale, CA, 2000.

[8] Smits, A. J., *A Physical Introduction to Fluid Mechanics*, Wiley, New York, 2000, p. 255.

[9] Crowe, C. T., Roberson, J. A., and Elger, D. F., *Engineering Fluid Mechanics*, 7th ed., Wiley, New York, 2001, p. 321.